OPTIMIZE YOUR SRS/SBRT QA

WITH SUB-MILLIMETER ACCURACY

ISOCENTER OPTIMIZATION ROUTINE

RIT software features an automated 3D Winston-Lutz Isocenter Optimization routine to give you a fast and precise measurement of isocenter accuracy. Using only a set of EPID Winston-Lutz images, the RIT system will calculate deviations between radiation and mechanical isocenter, determine ball/BB setup error, and suggest couch alignment adjustments to maximize your system's accuracy.

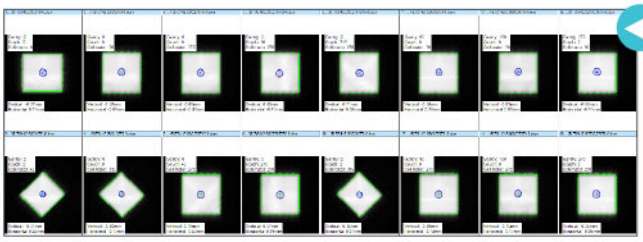

Automatically process a range of 3 to 16 EPID Winston-Lutz images for fast, sub-millimeter level accuracy of isocenter position. The routine allows physicists to perform daily or patient-specific analyses using specific clinical treatment angles with a ball setup error reported for each test. In addition to performing a full system analysis, you can perform partial system analyses and generate results with as few as 3 images.

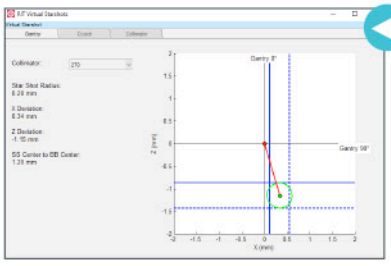

Eliminate your need for films and increase your accuracy using RIT's patented Virtual Star Shot feature with any combination of angles, reconstructed using a set of Winston-Lutz images in its dedicated window.

Patents: US 9192784, JP 6009705, CA 2918045, and other international patents pending.

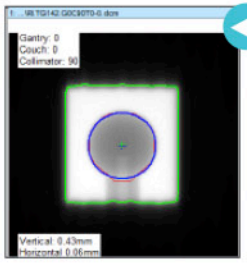

RIT's Isocenter Optimization routine allows for optimal cone detection, resulting in sub-pixel precision.

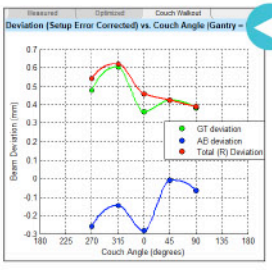

The Couch Walkout Plot displays beam deviation vs. couch rotation angle, which is a significant enhancement for customers adjusting the couch angle.

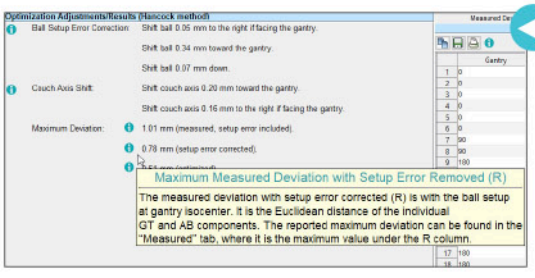

Information icons present clear and easy annotations to guide you through the advanced analysis.

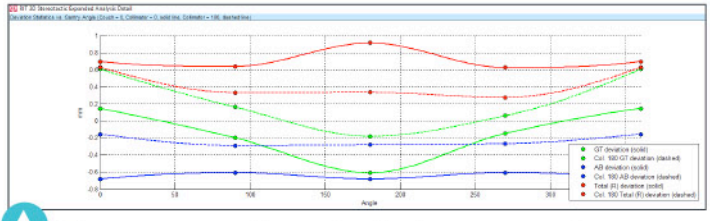

The routine enables individual component (gantry, collimator, couch) characterization to better understand distinct contributions to isocenter deviation, giving insight into adjustments that can be made to improve delivery performance, if needed.

CLICK TO VISIT **RADIMAGE.COM** TODAY TO DEMO THIS ADVANCED ROUTINE FROM RADIOLOGICAL IMAGING TECHNOLOGY, INC.

+1(719)590-1077, OPT. 4

SALES@RADIMAGE.COM

Connect with us on social media

RIT®

Received: 4 January 2022 | Revised: 12 May 2022 | Accepted: 8 July 2022

DOI: 10.1002/mp.15905

RESEARCH ARTICLE

MEDICAL PHYSICS

Construction of a digital fetus library for radiation dosimetry

Shuiyin Qu[1] | **Tianwu Xie**[1,2] | **Maryellen L. Giger**[3] | **Xianqing Mao**[4] | **Habib Zaidi**[2,5,6,7]

[1]Institute, of Radiation Medicine, Fudan University, Shanghai, China

[2]Division of Nuclear Medicine and Molecular Imaging, Geneva University Hospital, Geneva, Switzerland

[3]Department of Radiology, Committee on Medical Physics, University of Chicago, Chicago, Illinois, USA

[4]Faculty of Science, Technology and Medicine (FSTM), Department of Life Sciences and Medicine, University of Luxembourg, Esch-sur-Alzette, Luxembourg

[5]Geneva Neuroscience Center, Geneva University, Geneva, Switzerland

[6]Department of Nuclear Medicine and Molecular Imaging, University of Groningen, University Medical Center Groningen, Groningen, The Netherlands

[7]Department of Nuclear Medicine, University of Southern Denmark, Odense, Denmark

Correspondence
Tianwu Xie, Institute of Radiation Medicine, Fudan University, 2094 Xietu Road, Shanghai 200032, China.
Email: tianwuxie@fudan.edu.cn

Funding information
the Key Laboratory of Biomedical Engineering of Hainan Province under Opening Foundation, Grant/Award Number: 2022001; the Swiss National Science Foundation, Grant/Award Number: 320030_176052

Abstract

Purpose: Accurate estimations of fetal absorbed dose and radiation risks are crucial for radiation protection and important for radiological imaging research owing to the high radiosensitivity of the fetus. Computational anthropomorphic models have been widely used in patient-specific radiation dosimetry calculations. In this work, we aim to build the first digital fetal library for more reliable and accurate radiation dosimetry studies.

Acquisition and validation methods: Computed tomography (CT) images of abdominal and pelvic regions of 46 pregnant females were segmented by experienced medical physicists. The segmented tissues/organs include the body contour, skeleton, uterus, liver, kidney, intestine, stomach, lung, bladder, gall bladder, spleen, and pancreas for maternal body, and placenta, amniotic fluid, fetal body, fetal brain, and fetal skeleton. Nonuniform rational B-spline (NURBS) surfaces of each identified region was constructed manually using 3D modeling software. The Hounsfield unit values of each identified organs were gathered from CT images of pregnant patients and converted to tissue density. Organ volumes were further adjusted according to reference measurements for the developing fetus recommended by the World Health Organization (WHO) and International Commission on Radiological Protection. A series of anatomical parameters, including femur length, humerus length, biparietal diameter, abdominal circumference (FAC), and head circumference, were measured and compared with WHO recommendations.

Data format and usage notes: The first fetal patient-specific model library was developed with the anatomical characteristics of each model derived from the corresponding patient whose gestational age varies between 8 and 35 weeks. Voxelized models are represented in the form of MCNP matrix input files representing the three-dimensional model of the fetus. The size distributions of each model are also provided in text files. All data are stored on Zenodo and are publicly accessible on the following link: https://zenodo.org/record/6471884.

Potential applications: The constructed fetal models and maternal anatomical characteristics are consistent with the corresponding patients. The resulting computational fetus could be used in radiation dosimetry studies to improve the reliability of fetal dosimetry and radiation risks assessment. The advantages of NURBS surfaces in terms of adapting fetal postures and positions enable us to adequately assess their impact on radiation dosimetry calculations.

KEYWORDS
computational model, CT, fetus, pregnant patients, radiation dose

Shuiyin Qu and Tianwu Xie contributed equally to the work.

1 | INTRODUCTION

Accurate estimation of absorbed dose from ionizing radiation has always been a public health concern.[1] Pregnant females are part of the most vulnerable group of patients concerned by exposure to ionizing radiation owing to the high radiosensitivity of the fetus.[2–4] Potential scenarios where the fetus would be unfortunately exposed to ionizing radiation refer to medical exposure,[5,6] atomic bomb survivors,[7] airline passengers,[8] and professionally exposed staff.[4] According to the National Council on Radiation Protection and Measurements Report no 184,[9] in addition to background radiation, the major source of ionizing radiation exposure of the American public is related to the medical exposure. Pregnant females might be exposed to different sources of ionizing radiation, including diagnostic radiology,[1,10–12] radiation therapy,[13,14] and nuclear medicine[3,15–17] procedures. The health effects of ionizing radiation on the embryo/fetus depend on their gestational age: (i) The stage of 3–4 weeks of pregnancy is supposed to be the most likely period to suffer embryo death; (ii) whereas the pregnancy at 8–15 weeks is considered to be the most sensitive for radiation risks of growth retardation, microcephaly, and severe mental disability[18–20]; (iii) finally, at 16–40-week gestation, fetal radiation exposure higher than 1.5 Gy can result in both growth and mental retardation.[19,20] Biological damage caused by hazardous effects may occur sometimes after radiation exposure, potentially leading to cancer or mutations.[18] To reduce radiation risks, radiation exposure should be controlled as low as possible to reduce the fetal dose. As referred to some clinical indications (e.g., the diagnosis of pulmonary embolism), the benefit gained from radiological imaging to pregnant patients should be significantly higher than the associated radiation risks.[21] Therefore, accurate estimation of fetal radiation dose is highly desired. Direct measurement of the radiation dose delivered to patients from radiological imaging procedures is challenging but not impossible. A well-established alternative is to use Monte Carlo simulations for radiation transport performed using realistic anthropomorphic computational models.[5,22]

The development of computational models has gone through three generations, namely, stylized phantoms starting from the 1960s, voxel-based phantoms starting from the 1990s, and boundary representation (BERP)-based phantoms since 2000.[23–25] Several maternal and fetal phantoms have been developed using the three aforementioned generations. Stabin et al.[26] developed the first set of mathematical stylized pregnant women models. Computational phantoms based on the segmentation of patient imaging data are more realistic than stylized models. Angel et al.[21] constructed 24 patient-specific voxel phantoms of pregnant women. Nagaoka et al.[27] established a voxel phantom of pregnant women with realistic anatomical structures. However, in voxel models, organ deformation is not flexible enough, and the stepped structure may increase the surface area.[28] As a result, BERP models were proposed to enable more flexible organ deformation and posture change than voxel phantoms.[29] Xu et al.[30] developed the RPI models of pregnant females and fetuses at 3, 6, and 9 months of gestation, and they also evaluated fetal dose in computed tomography (CT) imaging,[31] specific absorption fractions (SAFs) (Φ_i) from the mother to fetal organs at different electron energies,[32] as well as SAFs for internal radiation dosimetry.[33] Hoseinian et al.[22] reported on hybrid reference phantom series of pregnant females with gestation ages of 3, 6, and 9 months derived from corresponding CT and MR images. Maynard et al.[34] developed a series of reference pregnant female models with gestational age of 8, 10, 15, 20, 30, 35, and 38 weeks. Xie and Zaidi[3] constructed eight maternal phantoms representing different gestational ages by adjusting the RPI models. However, the use of reference models may result in 66% overestimation or 77% underestimation of the fetal dose[35] as the impact of the individual fetal position is non-negligible in radiation dosimetry studies.[36] Therefore, the construction of more precise patient-specific computational models is undoubtedly meaningful and important for the reason of risk management and preventive health if we are willing to implement accurate radiation dosimetry for pregnant female patients.

The aim of this work is to construct a computational fetal library consistent with individual anatomical parameters extracted from CT images of actual patients. The developed patient-specific fetal phantom library has been used in the calculation of fetal organ radiation doses in our companion study.[37]

2 | ACQUISITION AND VALIDATION METHODS

2.1 | Image acquisition for pregnant patients

Imaging data of 46 pregnant patients were obtained from the Geneva University Hospital, Switzerland. These pregnant patients were referred to the emergency department of the hospital for abdominal and pelvic CT examinations. Pregnant patients came to the emergency department initially for acute abdominal pain and underwent ultrasound examination on admission. In the case that ultrasound examination did not allow us to draw any conclusive results or magnetic resonance imaging examination could not be carried out easily and immediately, the patients would be administrated a CT scan. The selected patients

TABLE 1 Fetal skull volume and organ scaling factor for the fetus model

Model number	Gestational age	Real age (weeks)	Skull volume (cm^3)	Organ scaling factor
Fetus_Model-20	Second trimester	17	81.16	0.87
Fetus_Model-21		18	69.56	0.83
Fetus_Model-22		20	103.84	0.94
Fetus_Model-23		20	110.59	0.96
Fetus_Model-24		21	108.22	0.96
Fetus_Model-25		21	105.64	0.95
Fetus_Model-26		22	158.39	1.09
Fetus_Model-27[a]		22	55.25	0.76
			70.59	0.83
Fetus_Model-28		23	189.73	1.15
Fetus_Model-29	Third trimester	25	496.89	1.59
Fetus_Model-30		25	192.30	1.16
Fetus_Model-31		25	374.02	1.45
Fetus_Model-32		25	210.74	1.19
Fetus_Model-33		26	274.59	1.30
Fetus_Model-34		26	223.03	1.22
Fetus_Model-35		28	273.87	1.30
Fetus_Model-36		29	273.87	1.30
Fetus_Model-37		29	366.26	1.44
Fetus_Model-38		29	341.77	1.40
Fetus_Model-39		30	340.73	1.40
Fetus_Model-40[b]		30	307.33	1.35
			356.84	1.42
Fetus_Model-41		32	410.69	1.49
Fetus_Model-42		33	404.25	1.48
Fetus_Model-43		33	387.77	1.46
Fetus_Model-44		35	500.16	1.59
Fetus_Model-45		35	417.70	1.50
Fetus_Model-46		35	582.73	1.68

[a]The first twins model at second trimester.
[b]The second twins model at third trimester.

are composed by 16 patients at first trimester of pregnancy, 12 patients of second trimester, and 18 of third trimester between 8 and 35 weeks of gestation. The fetal models were numbered consecutively Fetus_Model-1–46. Specific gestational age information of pregnant patients is provided in Table 1. CT imaging data of pregnant patients used in this study were acquired on one of the following CT scanners: General Electric (GE Medical Systems, Wisconsin) LightSpeed VCT, GE Discovery CT750 HD, Siemens Definition AS, Siemens SOMATOM Force (Siemens Healthineers, Forchheim, Germany), and Philips Brilliance 40 (Royal Philips, Amsterdam, the Netherlands). The final phantom length of each pregnant patient depends on the scan length of the CT scan that includes at least the anatomical structures from the lower chest to the pubic symphysis.

2.2 | Image segmentation

The desired anatomical structures were segmented by the combination of automatic thresholding-based and manual segmentations. The images were imported into Adobe Photoshop image processing software and the anatomical boundaries of body contours, skeleton, uterus, liver, kidney, intestine, stomach, lung, bladder, gall bladder, spleen, and pancreas for maternal body and the placenta, amniotic fluid, fetal body, fetal brain, and fetal skeleton for the conceptus manually segmented,

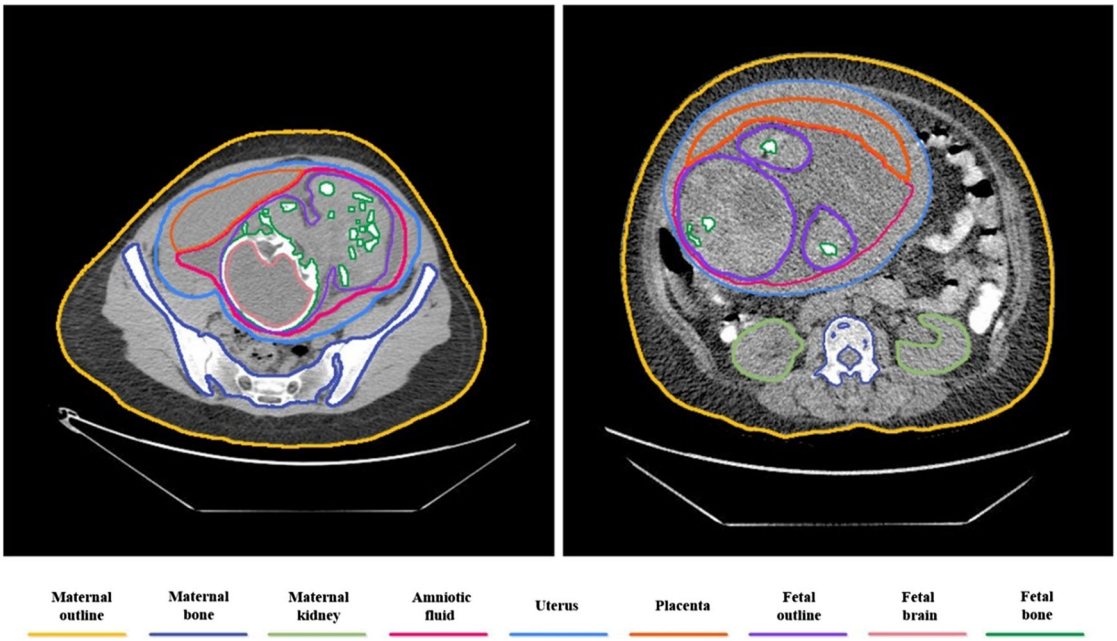

FIGURE 1 Segmentation of low-dose computed tomography (CT) images of pregnant patients into different tissue classes

as shown in Figure 1. The identified organs and tissues were reconstructed as polygon mesh models and imported into 3D modeling software for further processing.

2.3 | Construction of patient-specific fetal computable phantom

2.3.1 | Fetal skeleton models

The polygon mesh model of the fetal skeleton was imported into Rhinoceros software, where the nonuniform rational B-spline (NURBS) model is constructed from the polygon mesh model by lofting. As the scaffold of the human body, the structure of the skeleton determines the shape of the human body. In this study, the fetal skeleton was roughly divided into the following sites: skull, spine, ribs, clavicle, scapula, humerus, ulna, radius, hand bone, hip, femur, fibula, tibia, and foot bone. Before the construction of the fetal skeleton model, the previous parts were distinguished and saved in different layers.

In Rhinoceros, the basic workflow for surface reconstruction includes (i) drawing the outline of the polygonal mesh model of the fetal bone through the *Counter* command; (ii) using the *Rebuild* command to reconstruct the contour lines, while if necessary, the control points of organ contours can be deleted or modified to improve the smoothness of generated NURBS surfaces; and (iii) using the *Loft* command to construct the surface from the contours. The general process of making a NURBS model from a polygon mesh model is depicted in Appendix Figure 1. Additional operations may be needed for the construction of some individual parts. For the fetal skull, the mandible and other parts of the skull need to be constructed separately and combined by the *Join* command. For the fetal ribs, the *Pipe* command was used to generate a series of pipes to represent the ribs. For the fetal spine, the form of overlapping and intersecting vertebral segments was adopted for the generation of the whole spine. The two surfaces of the ilium and ischia, the ilium and the pubis, were constructed separately because of the obturator foramen of the hip, which then combined together to form the hip bone.

2.3.2 | Fetal organ models

The surface reconstruction process of the fetal brain is similar to what has been described in Section 2.3.1 whereas the spinal cord is constructed as a pipeline model inside the spine. The fetal organ constructed in this study was originally derived from a certain scale of the organ of the *Anchor* model, which has been constructed in previous work by our group.[3] The *Anchor* model uses advanced BERP geometry of NURBS and polygonal meshes consisting of 25 organs/tissues, whereas organ masses were adjusted carefully to match the reference data of International Commission on Radiological Protection (ICRP)[38] with differences less than 0.3%. Fetal organs of the esophagus, eyes, thyroid, lungs, heart, kidney, liver, stomach, gall bladder, salivary gland, large intestine, small intestine, urinary bladder, skin, ovaries, testis, adrenal, pancreas,

spleen, and thymus were constructed from the anchor phantom. Except the skeleton, brain, and spinal cord mentioned earlier, which were constructed separately, the detailed construction steps of the other fetal organs are described as follows:

Step 1: Calculation of organ scaling factor r reflecting the ratio of organ volume V_{ao} of the constructed fetal phantom to the corresponding organ volume V_{AO} of the anchor phantom, determined by the following formula:

$$r = \sqrt[3]{\frac{V_{ao}}{V_{AO}}} = \sqrt[3]{\frac{V_{as}}{V_{AS}}} \quad (1)$$

where V_{as} refers to the skull volume of the fetal phantom to be constructed, and V_{AS} refers to the skull volume of the anchor phantom. The organ scaling factor calculated by Equation (1) is shown in Table 1. After estimating organ scaling factors, the fetal organs were placed in the corresponding anatomical positions using rotation and displacement tools. The placement of the eyes is based on the position of the eye sockets in the polygonal mesh model of the skull.

Step 2: In the literature, the femoral length (FL) is often used for the estimation of the fetus weight.[39,40] In this work, we measured the fetal FL from the polygonal mesh model of the fetal skeleton. This process will be described in detail in Section 2.3.5. The 50 quartile FL reference value given in the World Health Organization (WHO) fetal growth charts[41] was fitted with the 50 quartile estimated fetal weight reference value (W) as

$$W = 47.612\ e^{0.0599 \times FL} \quad (2)$$

The estimated fetal weight of each computational fetal model was calculated. The measured FL values for each model are shown in Table 3. The reference mass of 11 fetal organs given in the ICRP Publication 89[38] were fitted with the reference fetal body weight. For organs lacking given reference masses at different gestational ages, the ratio for organ mass to body mass was calculated. The fitted correlations between organ mass and body mass are summarized in Appendix Table 1.

Step 3: The Hounsfield unit (HU) values of the maternal uterus, placenta, amniotic fluid, fetal brain, fetal soft tissue, fetal liver, fetal bone cortex, and fetal bone marrow were measured using the ImageJ software package.[1] Regions of interest were defined, as shown in Appendix Figure 2, to calculate the average HU and, hence, tissue density according to the formula given by Schneider et al.[42] The obtained density at the same gestational period was averaged.

Step 4: The fetal organ models were scaled to meet the target volume, whereas the organ position was

[1] https://imagej.nih.gov/

TABLE 2 Density measurements (in g/cm^3) from computed tomography (CT) images

Organ/tissue	Gestational age (month)								
	2	3	4	5	6	7	8	9	
Uterine wall	1.052[a]	1.052	1.052	1.052 ± 0.012	1.052 ± 0.009	1.052 ± 0.007	1.052 ± 0.005	1.052 ± 0.006	
Amniotic fluid	1.022 ± 0.023	1.022 ± 0.010	1.022 ± 0.003	1.022 ± 0.049	1.022 ± 0.018	1.022 ± 0.004	1.022 ± 0.015	1.022 ± 0.045	
Fetal soft tissue	1.020 ± 0.013	1.020 ± 0.021	1.053 ± 0.005	1.053 ± 0.002	1.053 ± 0.002	1.053 ± 0.002	1.053 ± 0.002	1.053 ± 0.002	
Fetal skeleton	1.058	1.125	1.185 ± 0.004	1.264 ± 0.009	1.316 ± 0.015	1.407 ± 0.009	1.475 ± 0.007	1.509 ± 0.006	
Fetus bone marrow	0.966	1.038	1.097 ± 0.023	1.141 ± 0.017	1.188 ± 0.046	1.201 ± 0.018	1.209 ± 0.049	1.216 ± 0.031	
Fetus brain	1.020	1.020	1.030	1.030 ± 0.025	1.030	1.030 ± 0.027	1.030 ± 0.038	1.030 ± 0.038	
Fetus liver	1.020	1.020	1.062 ± 0.004	1.062 ± 0.000	1.062 ± 0.002	1.062 ± 0.001	1.062 ± 0.000	1.062 ± 0.000	

[a]Some values in the table have no standard deviation owing to the poor quality of low-dose CT images and the inability to distinguish fetal tissues.

TABLE 3 Measurements of anatomical parameters (in mm) for the developing fetus

Gestational age (week)	Sample size	Femur length	Humerus length	Biparietal diameter	Head circumference	Fetus abdominal circumference
8	11	–	–	–	–	–
10	3	–	–	8.88 (8.69, 9.09)	33.09 (32.82, 33.45)	–
12	2	–	–	9.13 (9.11, 9.15)	33.06 (32.71, 33.40)	–
15	2	30.72 (30.67, 30.76)	29.13 (29.13, 29.13)	37.46 (36.97, 37.95)	133.50 (132.90, 134.10)	–
16	1	32.88	31.31	37.34	133.50	–
17	1	32.58	31.37	46.91	171.00	151.60
18	1	30.97	29.91	48.64	162.80	148.90
20	2	34.58 (34.23, 34.93)	34.04 (33.33, 34.75)	52.45 (51.65, 53.25)	184.50 (175.90, 193.10)	195.95 (189.30, 202.60)
21	2	33.98 (31.92, 36.04)	33.78 (32.94, 34.62)	52.43 (52.15, 52.70)	186.25 (184.4, 188.1)	168.60 (158.00, 179.20)
22[a]	2	34.05 (27.88, 42.87)	31.11 (26.01, 39.84)	52.17 (43, 64.51)	178.77 (153.88, 218.79)	185.15 (168.70, 202.10)
23	1	46.64	43.25	68.00	233.20	229.60
25	4	55.00 (45.82, 68.97)	50.51 (39.48, 64.31)	77.7 (63.81, 94.13)	271.58 (230.90, 321.80)	275.83 (233.90, 349.20)
26	1	53.40	46.37	71.31	253.30	229.85
28	1	55.96	51.31	76.38	263.50	242.80
29	2	59.54 (56.15, 62.93)	53.52 (48.33, 58.70)	80.79 (78.33, 83.24)	284.00 (278.70, 289.30)	260.40 (256.70, 264.10)
30[b]	2	59.03 (57.66, 61.75)	52.62 (51.21, 54.75)	82.38 (76.67, 87.91)	283.22 (272.23, 291.78)	240.90 (230.77, 257.36)
32	1	64.51	61.12	88.30	309.30	278.30
33	2	61.06 (60.91, 61.2)	55.62 (55.62, 55.62)	85.35 (85.05, 85.65)	295.75 (295.30, 296.20)	242.15 (239.80, 244.50)
35	3	68.72 (65.95, 72.68)	56.92 (55.79, 58.31)	90.1 (84.75, 97.02)	325.03 (311.70, 341.54)	323.17 (309.20, 332.60)

[a]The first twin fetus model at second trimester.
[b]The second twin fetus model at third trimester.

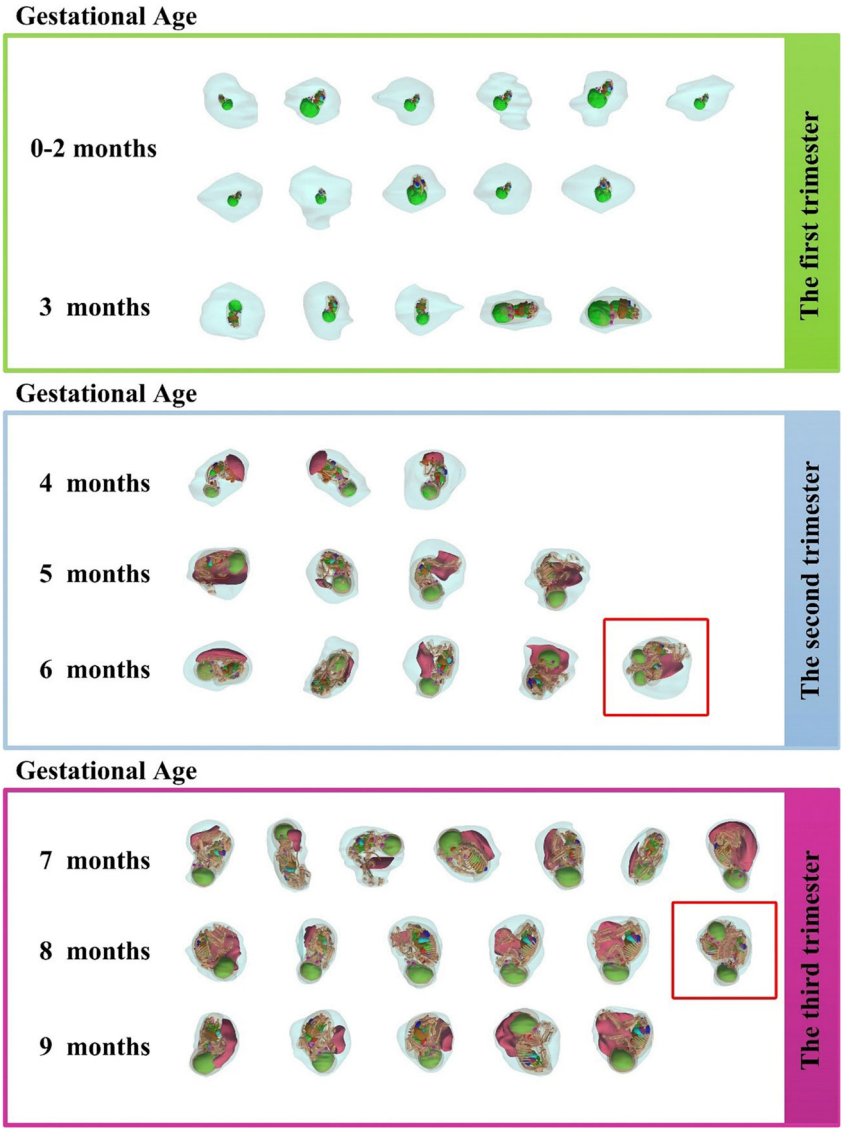

FIGURE 2 3D visualization of the fetal models in the first, second, and third trimesters. (Green for fetal brain, pink for placenta, blue for uterus, whereas the red boxes correspond to two twin models)

carefully adjusted to avoid overlap and to ensure that the organs remain inside the chest and abdominal cavity.

2.3.3 | Maternal abdominal model

Based on the constructed polygonal mesh models of the maternal body and other organs, the models of maternal abdomen and internal organs were constructed following identical procedures to those described in Section 2.3.1.

2.3.4 | Fetal models at 8–16 weeks

The fetus is invisible in low-dose CT images of pregnant patients at gestational age between 8 and 16 weeks. The crown-rump length, defined as the distance between the top of the head and the lowest buttocks of the fetus, is less than 24 mm for fetuses younger than 16-week gestational age.[43] For pregnant patients at this gestational period, we only segmented maternal structures and the uterus, whereas the "Anchor" models of 8- and 16-week gestational ages were scaled according to the corresponding ICRP reference fetal weights for the construction of fetus models.

2.3.5 | Measurement of fetal anatomical parameters

After the construction of the computational fetus library, the anatomical parameters of the fetus, such as FL, humerus length (HL), biparietal diameter (BPD), head circumference (HC), and abdominal circumference (FAC), were further measured. To ensure the authenticity and accuracy of the implemented measurements, FL

and HL were measured on the polygonal mesh model of the femur and humerus, whereas HC, BPD and FAC were measured on the reconstructed NURBS surface to avoid the measurement errors introduced by the stepped shape of skull and fetal contour segmentations.

2.3.6 | Phantom evaluation

To evaluate the realism and accuracy of the constructed fetal phantom library, the measured fetal anatomical parameters and organ masses were compared with the reference values of the ICRP publication 89[38] and the WHO report.[41] The relationship between the reference values of fetal anatomical parameters given in WHO and gestational weeks was fitted, whereas the measured values reported in this study were plotted on the same map in the form of scattered data for comparison. In addition, the maximum, minimum, and median of organ masses of 46 developed phantoms were calculated and compared with the corresponding reference values given by ICRP publication 89.

3 | DATA FORMAT AND USAGE NOTES

3.1 | Computational fetus library for pregnant female and fetus

A computational fetus library was constructed, including 46 fetus models with gestational age ranging from 8 to 35 weeks. It takes about 4 days to construct one fetal model. The visualization of 3D images of the developed fetus models (including uterus and placenta) at the second and third trimester are shown in Figure 2. The computational fetus of Fetus_Model-25 and Fetus_Model-39 are shown in Figure 3. The fetal skin model with eyes, fetal organ model, except the skin, and the fetal skeleton model of fetus Fetus_Model-46 are illustrated in Figure 4.

All generated models have been voxelized and uploaded to the Zenodo collection that is publicly accessible using the following link: https://zenodo.org/record/6471884. The voxelized models are provided as MCNPX input files, which are text files composed of 2D array of integers corresponding to the fetal tissues and maternal organs. The voxel size, matrix dimension, and material definitions are specified, whereas all models are centered on the source-to-isocenter distance in both *x*–*y* plane and *z* direction.

3.2 | Fetal organs density

The density of the fetal skeleton changes significantly across different gestational ages.[44,45] In the current study, the density of the fetal skeleton for each individual patient was calculated by measuring the HUs on CT images and averaging them at each age of pregnancy. The organs considered for density measurement include amniotic fluid, placenta and fetal bones, bone marrow, brain, liver, and soft tissue. Table 2 lists the adopted organ density for the fetus, whereas the density of other fetal organs is set similar to fetal soft-tissue. The maternal organ/tissue listed in Table 2, such as placenta and amniotic fluid, their densities were calculated from HUs measured on CT images, whereas the density of other organs/tissues, such as skin and uterine wall, was determined according to ICRP publication 89.[38] The density of fetal skeleton and bone marrow increases gradually with increasing gestational age. The average density of the fetal skeleton is 1.058 and 1.509 g/cm^3 in the 2nd and 9th month, respectively.

3.3 | Anatomical characteristics of the fetus

The anatomical parameters of the computational models were measured to investigate the correlation between the anatomical characteristics and radiation dosimetry calculations. The minimum BPD is 8.69 mm, whereas the maximum BPD is 97.02 mm. The measured FL, HL, HC, and FAC of the fetus ranges from 27.88 to 72.68 mm, from 26.01 to 64.31 mm, from 32.71 to 341.54 mm, and from 148.9 to 349.2 mm, respectively. The average values of BPD, FL, HL, HC, and FAC are 60.42, 49.05, 45.13, 212.08, and 236 mm, respectively. The measured anatomical parameters are listed in Table 3, whereas Figure 5 compares the measurements of FL, HL, HC, BPD, and FAC with reference values reported by WHO.[41] The estimated fetal weight calculated by Equation (2) was also compared. The black line is the quadratic fitting curve of the 50-percentile reference value obtained from the WHO report, whereas the red data points represent the measured value for each individual fetus. The mean differences of FL, HL, BPD, HC, abdominal circumference, and estimated fetal weight between the measured values and corresponding quadratic fitting curve of WHO were 18%, 17%, 13%, 9%, 14%, and 47%, respectively. The anatomical characteristics of the developed models fit well with the recommendations of WHO with a coherent trend, hence reflecting the anatomical reliability of the constructed models.

3.4 | Fetal organ masses

Fetal organ masses were estimated for each model. Figure 6 shows the median, maximum, and minimum values of fetal weight and fetal organ mass of the brain, thyroid, heart, adrenal gland, spinal cord, kidney, liver, lung, pancreas, spleen, and thymus. The reference

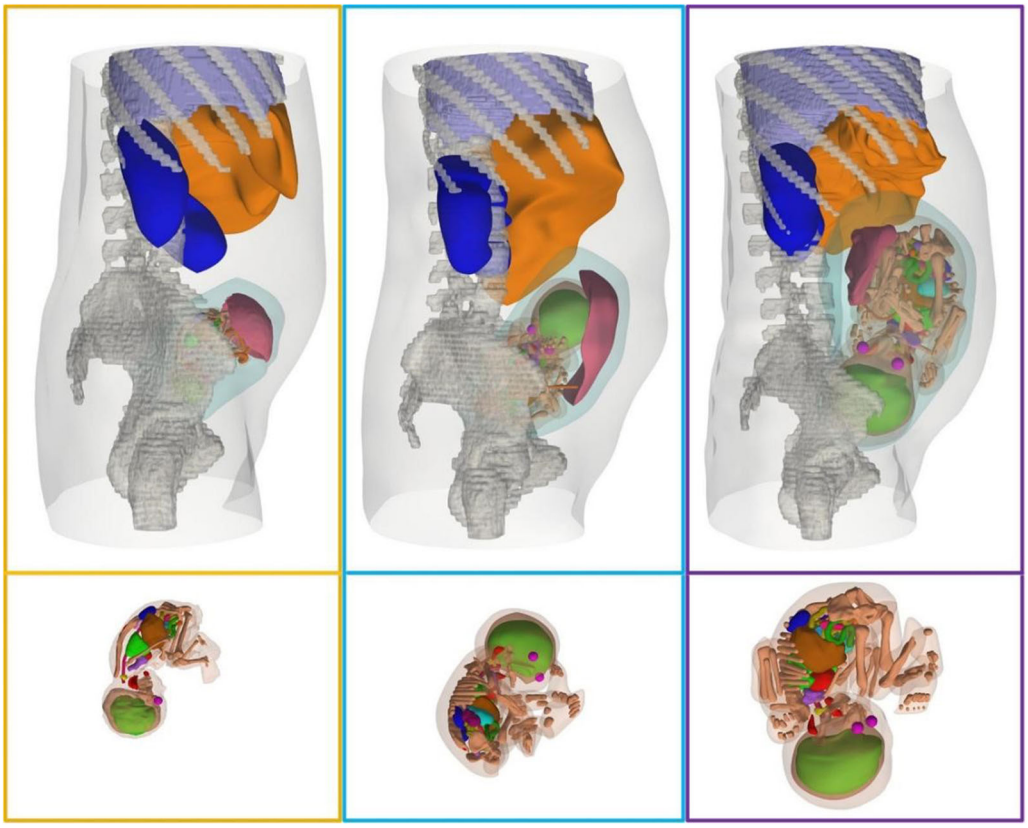

FIGURE 3 3D visualization of maternal phantoms (first row) at the second trimester (left) and third trimester (right) with their corresponding fetus models (second row)

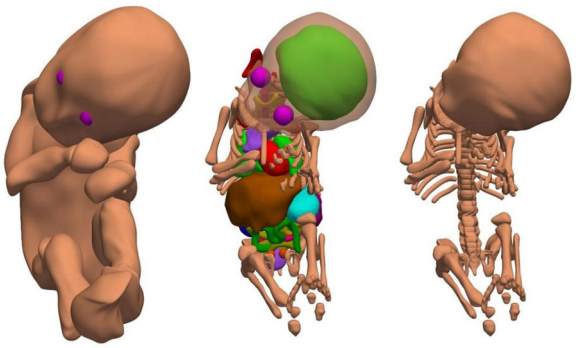

FIGURE 4 Surface rendering of 35-week-old fetus with (a) the skin model, (b) the organ model, and (c) the skeleton model

values given by ICRP publication 89[38] were also used for comparison. For most cases, there was a good agreement between the organ masses reported in this work and ICRP reference values.

4 | DISCUSSION

We constructed the first computational fetus library consisting of 46 models with gestational age ranging from 8 to 35 weeks. The developed fetal models include 25 identified organs/tissues. Their volumes were carefully adjusted to match the reference volume, whereas the HU measurements were used to determine corresponding organ/tissue densities. The phantom library was constructed based on real clinical CT images with the contour and skeleton of the model, size, position, and posture of the fetus being consistent with scanned patients. The density of fetal organs was calculated based on measured HUs from CT images, which provides better authenticity than ICRP reference values. To the best of our knowledge, the fetuses in reported reference pregnant phantoms are mostly at head-down position, thus failing to represent the changing posture and position of the fetuses in pregnant women at different gestational ages, which may introduce errors for dose assessment and radiation risk analysis for the developing fetuses. The generated NURBS model is suitable for deformation and displacement, thus enabling us to study the effect of conceptus position and fetal posture on radiation dosimetry calculations.

The organ masses of the computational fetus library are in good agreement with reference values of ICRP publication 89,[38] whereas the anatomical parameters of the developing fetus show a coherent trend with the values reported by WHO.[41] The measured parameters of the developed models are slightly higher than the reported values of WHO, and this may be attributed

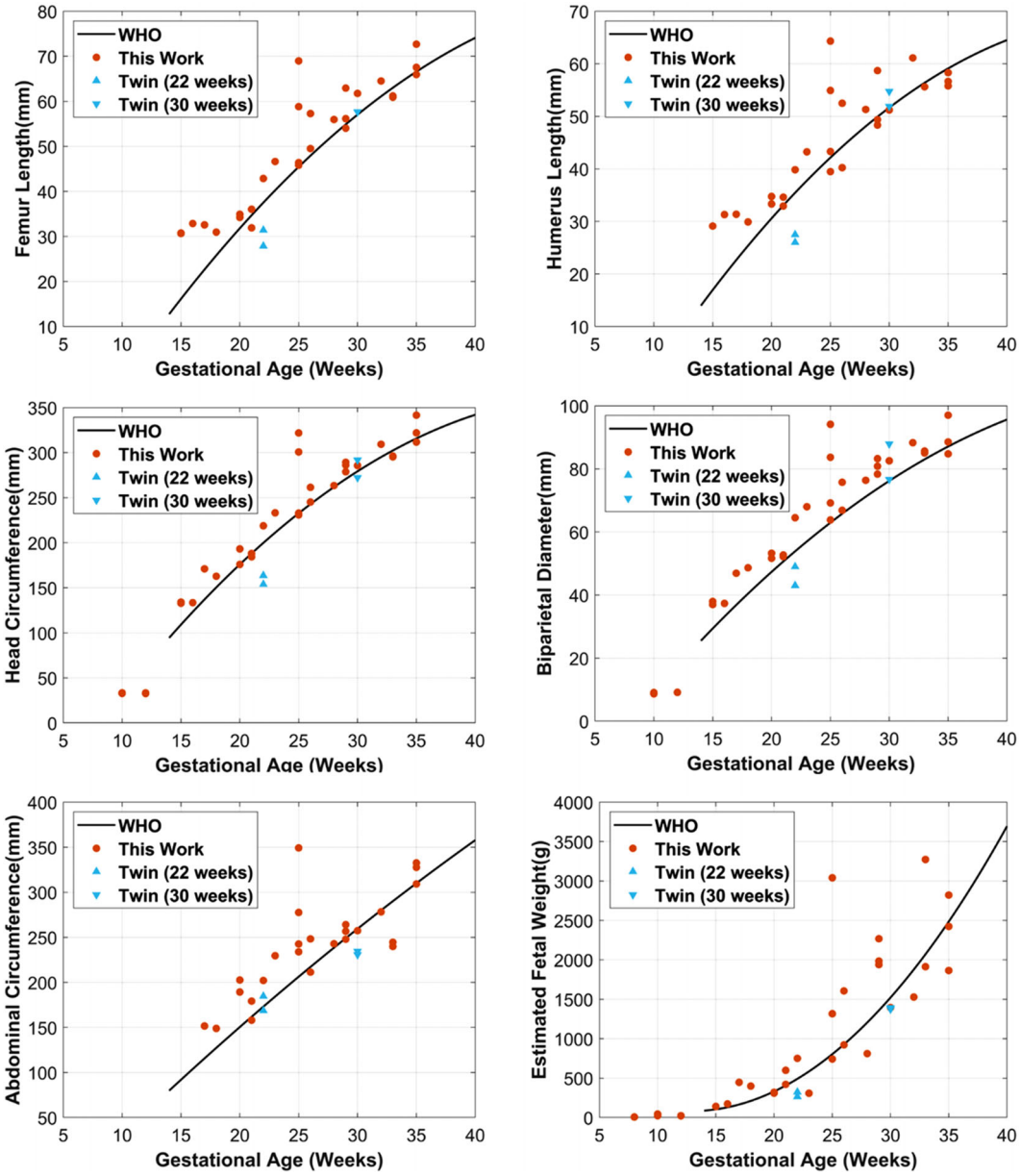

FIGURE 5 Comparison of anatomical parameters between this work and the reference values reported in World Health Organization (WHO) report. The red data points refer to measured values in this work, whereas the solid line represents the fitting curve of WHO data.

to the different subject populations (one hospital in a single country for this study vs. three ethnic groups for WHO). The constructed computational fetus library provides more accurate representation of anatomical changes for the developing fetus. With increasing concerns related to radiological imaging of pregnant patients, this library provides a precious tool for radiation dosimetry and radiation protection research on pregnant patients. The developed computational fetus library will be made available to the scientific community for academic use.

This study bears inherently a number of limitations. The segmentation of fetal organs was performed on low-dose CT images where image noise and ambiguity might introduce additional errors to the segmentation results, including unrecognized or over-recognized regions of identified tissues. Although the constructed library included the largest state-of-the-art developing fetus group with gestational age ranging from 8 to 35 weeks, additional data from other regions/countries would be highly appreciated to compensate variability existing in the current patient population.

5 | CONCLUSION

The developed digital fetus library will be used for radiation dosimetry studies directed toward risk-benefit

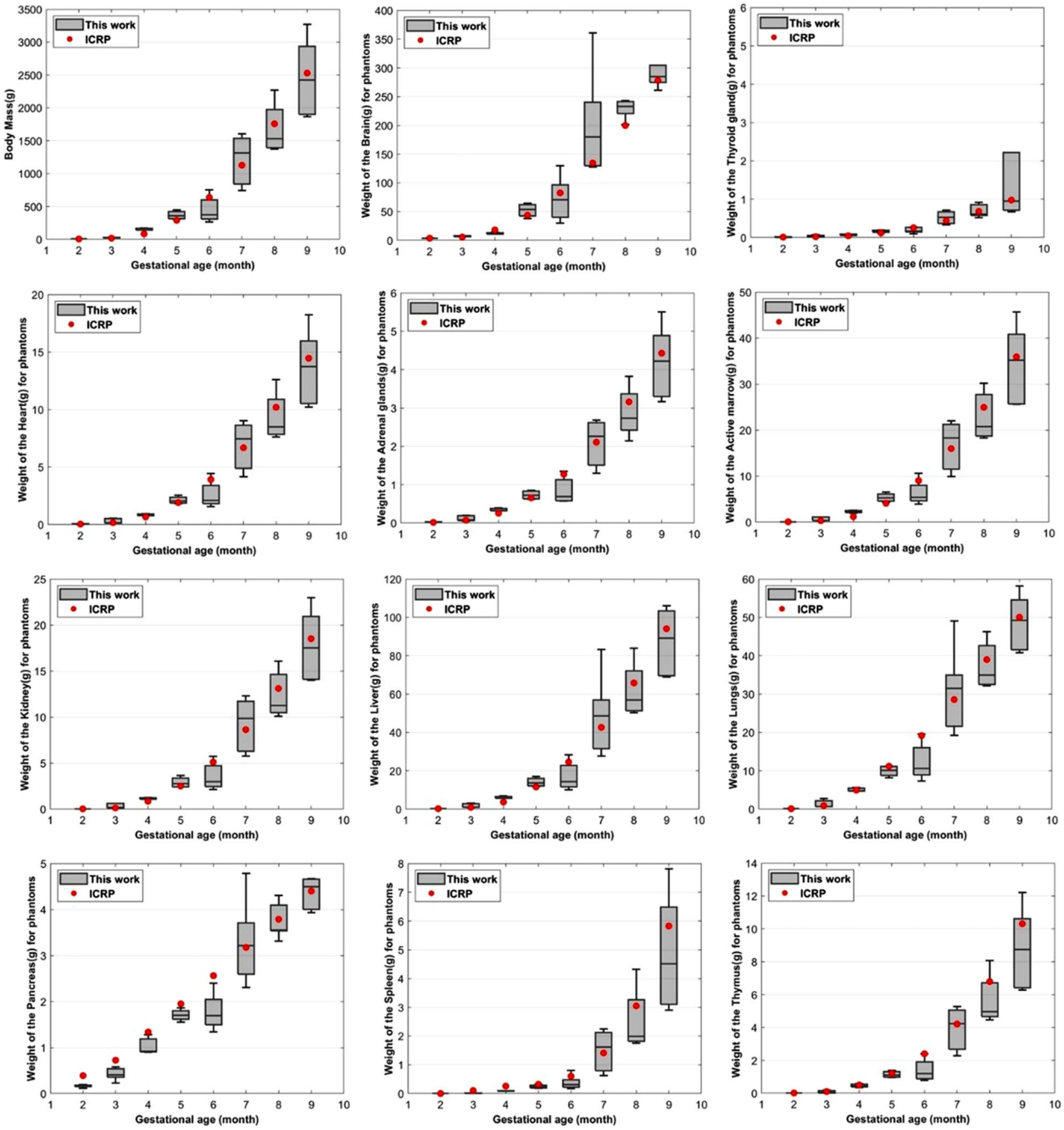

FIGURE 6 Comparison of fetal organ mass between models developed in this work and the International Commission on Radiological Protection (ICRP) reference values

analysis for pregnant females receiving abdominal and pelvic CT examinations. The characteristics of NURBS surfaces make them suitable to generate new models through deformation and displacement, which enable our understanding on the effect of fetal postures and positions on radiation dose calculations in various scenarios. Such studies are expected to pave the way for building a comprehensive radiation dosimetry framework for de-risking pregnant patients undergoing radiological examinations.

ACKNOWLEDGMENTS

This work was supported by the Key Laboratory of Biomedical Engineering of Hainan Province under Opening Foundation 2022001 and the Swiss National Science Foundation under Grant no. SNSF 320030_176052.

CONFLICT OF INTEREST

The authors declare that there are no conflict of interests about this work.

REFERENCES

1. Osei EK, Faulkner K. Fetal doses from radiological examinations. *Br J Radiol*. 1999;72(860):773-780.
2. ICRP. Publication 84: pregnancy and medical radiation. Ann ICRP. 2000;30:1-62.
3. Xie T, Zaidi H. Development of computational pregnant female and fetus models and assessment of radiation dose from positron-emitting tracers. *Eur J Nucl Med Mol Imaging*. 2016;43(13):2290-2300.
4. Osei EK, Kotre CJ. Equivalent dose to the fetus from occupational exposure of pregnant staff in diagnostic radiology. *Br J Radiol*. 2001;74(883):629.
5. Xie T, Poletti PA, Platon A, Becker CD, Zaidi H. Assessment of CT dose to the fetus and pregnant female patient using patient-specific computational models. *Eur Radiol*. 2018;28(3):1054-1065.
6. Lazarus E, Debenedectis C, North D, Spencer PK, Mayo-Smith WW. Utilization of imaging in pregnant patients: 10-year review of 5270 examinations in 3285 patients—1997–2006. *Radiology*. 2009;251(2):517-524.
7. Paulbeck C, Griffin K, Lee C, et al. Dosimetric impact of a new computational voxel phantom series for the Japanese atomic bomb survivors: pregnant females. *Radiat Res*. 2019;192(5):538-561.
8. Magann EF, Chauhan SP, Dahlke JD, McKelvey SS, Watson EM, Morrison JC. Air travel and pregnancy outcomes: a review of pregnancy regulations and outcomes for passengers, flight attendants, and aviators. *Obstet Gynecol Surv*. 2010;65(6):396-402.
9. NCRP. NCRP Report No. 184 – Medical Radiation Exposure of Patients in the United States (2019). 2019.
10. Gilet AG, Dunkin JM, Fernandez TJ, Button TM, Budorick NE. Fetal radiation dose during gestation estimated on an anthropomorphic phantom for three generations of CT scanners. *Am J Roentgenol*. 2011;196(5):1133-1137.
11. Kelaranta A, Kaasalainen T, Seuri R, Toroi P, Kortesniemi M. Fetal radiation dose in computed tomography. *Radiat Prot Dosim*. 2015;165(1-4):226-230.
12. Damilakis J, Perisinakis K, Tzedakis A, Papadakis AE, Karantanas A. Radiation dose to the conceptus from multidetector CT during early gestation: a method that allows for variations in maternal body size and conceptus position. *Radiology*. 2010;257(2):483-489.
13. Mazonakis M, Damilakis J. Estimation and reduction of the radiation dose to the fetus from external-beam radiotherapy. *Physica Med*. 2017;43:148-152.
14. Makkia R, Nelson K, Zaidi H, Dingfelder M. Construction of realistic hybrid computational fetal phantoms from radiological images in three gestational ages for radiation dosimetry applications. *Phys Med Biol*. 2019;64(20):205003.
15. Zanotti-Fregonara P, Chastan M, Edet-Sanson A, et al. New fetal dose estimates from ^{18}F-FDG administered during pregnancy: standardization of dose calculations and estimations with voxel-based anthropomorphic phantoms. *J Nucl Med*. 2016;57:1760-1763.
16. Xie T, Zanotti-Fregonara P, Edet-Sanson A, Zaidi H. Patient-specific computational model and dosimetry calculations for a patient pregnant with twins undergoing a PET/CT examination. *J Nucl Med*. 2018;59(9):1451-1458.
17. Xie T, Zaidi H. Fetal and maternal absorbed dose estimates for positron-emitting molecular imaging probes. *J Nucl Med*. 2014;55(9):1459-1166.
18. Santis MD, Gianantonio ED, Straface G, et al. Ionizing radiations in pregnancy and teratogenesis: a review of literature. *Reprod Toxicol*. 2005;20(3):323-329.
19. Stabin, MG. Radiation dose concerns for the pregnant or lactating patient. *Semin Nucl Med*. 2014;44(6):479-488.
20. Dauer LT, Thornton RH, Miller DL, et al. Radiation management for interventions using fluoroscopic or computed tomographic guidance during pregnancy: a joint guideline of the society of interventional radiology and the cardiovascular and interventional radiological society of europe with endorsement by the Canadian Interventional Radiology Association. *J Vasc Intervent Radiol: JVIR*. 2012;23(1):19-32.
21. Angel E, Wellnitz CV, Goodsitt MM, et al. Radiation dose to the fetus for pregnant patients undergoing multidetector CT imaging: Monte Carlo simulations estimating fetal dose for a range of gestational age and patient size1. *Radiology*. 2008;249(1):220-227.
22. Hoseinian E, Motavalli LR, Hakimabad HM. Hybrid pregnant reference phantom series based on adult female ICRP reference phantom. *Radiat Phys Chem*. 2018;144:386-395.
23. Xu XG. An exponential growth of computational phantom research in radiation protection, imaging, and radiotherapy: a review of the fifty-year history. *Phys Med Biol*. 2014;59(18):R233-R302.
24. Zaidi H, Tsui BMW. Review of computational anthropomorphic anatomical and physiological models. *Proc IEEE*. 2009;97(12):1938-1953.
25. Kainz W, Neufeld E, Bolch WE, et al. Advances in computational human phantoms and their applications in biomedical engineering—a topical review. *IEEE Trans Radiat Plasma Med Sci*. 2019;3(1):1-23.
26. Stabin MG, Cristy M, Ryman J C, et al. *Mathematical Models and Specific Absorbed Fractions of Photon Energy in the Nonpregnant Adult Female and at the End of Each Trimester of Pregnancy*. Oak Ridge National Laboratory; 1995.
27. Nagaoka T, Togashi T, Saito K, Takahashi M, Ito K, Watanabe S. An anatomically realistic whole-body pregnant-woman model and specific absorption rates for pregnant-woman exposure to electromagnetic plane waves from 10 MHz to 2 GHz. *Phys Med Biol*. 2007;52(22):6731-6745.
28. Caon M. Voxel-based computational models of real human anatomy: a review. *Radiat Environ Biophys*. 2004;42(4):229-235.
29. Choi C, Yeom YS, Lee H, et al. Body-size-dependent phantom library constructed from ICRP mesh-type reference computational phantoms. *Phys Med Biol*. 2020;65(12):125014.
30. Xu XG, Taranenko V, Zhang J, Shi C. A boundary-representation method for designing whole-body radiation dosimetry models: pregnant females at the ends of three gestational periods—RPI-P3, -P6 and -P9. *Phys Med Biol*. 2007;52(23):7023-7044.
31. Gu J, Xu XG, Caracappa PF, Liu B. Fetal doses to pregnant patients from CT with tube current modulation calculated using Monte Carlo simulations and realistic phantoms. *Radiat Prot Dosim*. 2013;155(1):64-72.
32. Guo B, Xu XG, Shi C. Specific absorbed fractions for internal electron emitters derived for a set of anatomically realistic reference pregnant female models. *Radiat Prot Dosim*. 2009;138:20-28.
33. Taranenko V, Xu XG. Fluence-to-absorbed-dose conversion coefficients for neutron beams from 0.001 eV to 100 GeV calculated for a set of pregnant female and fetus models. *Phys Med Biol*. 2008;53(5):1425-1446.
34. Maynard MR, Long NS, Moawad NS, et al. The UF family of hybrid phantoms of the pregnant female for computational radiation dosimetry. *Phys Med Biol*. 2014;59(15):4325-4343.
35. Osei EK, Faulkner K. Fetal position and size data for dose estimation. *Br J Radiol*. 1999;72(856):363-370.
36. Krstic D, Nikezic D. Efficiency of whole-body counter for various body size calculated by MCNP5 software. *Radiat Prot Dosim*. 2012;152:179–183.
37. Qu S, Xue M, Zaidi H, Xie T Patient-specific fetal radiation dosimetry for pregnant patients undergoing abdominal and pelvic CT imaging. *Med Phys*. in process.
38. ICRP. Publication 89: basic anatomical and physiological data for use in radiological protection: reference values. *Ann ICRP*. 2002;32(3):1-277.

39. Hill LM, Breckle R, Gehrking WC, O'Brien PC. Use of femur length in estimation of fetal weight. *Am J Obstet Gynecol*. 1985;152(7):847-852.
40. Campbell WA, Vintzileos AM, Neckles S, Weinbaum PJ, Nochimson DJ. Use of the femur length to estimate fetal weight in premature infants: preliminary results. *J Ultrasound Med*. 1985;4(11):583.
41. Kiserud T, Piaggio G, Carroli G, Widmer M, Platt LD. The World Health Organization fetal growth charts: a multinational longitudinal study of ultrasound biometric measurements and estimated fetal weight. *PLoS Med*. 2017;14(1):e1002220.
42. Schneider W, Bortfeld T, Schlegel W. Correlation between CT numbers and tissue parameters needed for Monte Carlo simulations of clinical dose distributions. *Phys Med Biol*. 2000;45(2):459.
43. Nardozza LMM, Nowak PM, Júnior EA, et al. Evaluation of placental volume at 7–10 + 6 weeks of pregnancy by 3D-sonography. *Placenta*. 2009;30:585-589.
44. Minton SD, Steichen JJ, Tsang RC. Bone mineral content in term and preterm appropriate-for-gestational-age infants. *J Pediatr*. 1979;95(6):1037-1042.
45. Mimouni F, Tsang RC. Bone mineral content: data analysis. *J Pediatr*. 1988;113(1 pt 2):178-180.

How to cite this article: Qu S, Xie T, Giger ML, Mao X, Zaidi H. Construction of a digital fetus library for radiation dosimetry. *Med Phys*. 2022;1-13. https://doi.org/10.1002/mp.15905

Platform

SunCHECK™

One Database for Complete Quality Management

Learn more >

Patient

- Plan Quality Checks
- Secondary Dose Calculations
- Pre-Treatment QA
- In-Vivo Monitoring

Machine

- Standardized Routine QA
- Direct Device Control
- Automated Imaging, MLC & VMAT QA
- Protocol-Based QA